Coupling of Spinons with Defects and Phonons in the Spin Chain Compound Ca_2CuO_3

Xi Chen,[1] Jesús Carrete,[2] Sean Sullivan,[1] Ambroise van Roekeghem,[3] Zongyao Li,[1] Xiang Li,[1] Jianshi Zhou,[1,4] Natalio Mingo,[3] and Li Shi[1,4,*]

[1]*Materials Science and Engineering Program, Texas Materials Institute, The University of Texas at Austin, Austin, Texas 78712, USA*

[2]*Institute of Materials Chemistry, TU Wien, A-1060 Vienna, Austria*

[3]*LITEN, CEA-Grenoble, 17 rue des Martyrs, 38054 Grenoble Cedex 9, France*

[4]*Department of Mechanical Engineering, The University of Texas at Austin, Austin, Texas 78712, USA*

(Received 17 November 2018; revised manuscript received 14 February 2019; published 6 May 2019)

Extrinsic spinon scattering by defects and phonons instead of intrinsic spinon-spinon coupling is responsible for resistive magnetic heat transport in one-dimensional (1D) quantum magnets. Here we report an investigation of the elusive extrinsic effect in the 1D Heisenberg $S = 1/2$ spin chain compound Ca_2CuO_3, where the defect concentration is determined from the measured specific heat and first-principles calculations are used to separate the lattice component of the measured thermal conductivity to isolate a large magnetic contribution (κ_m). The obtained temperature-dependent spinon-defect and spinon-phonon mean free paths can enable a quantitative understanding of both κ_m and the spinon-induced spin Seebeck effect.

DOI: 10.1103/PhysRevLett.122.185901

Quasi-one-dimensional (1D) magnetic spin systems exhibit a rich variety of physical phenomena, such as superconductivity [1], spin-orbital separation [2], the spin Seebeck effect (SSE) [3,4], and spin entanglement [5]. Among these 1D systems, the $S = 1/2$ Heisenberg spin chains with antiferromagnetic coupling between adjacent spins are of particular interest. The elementary spin excitations in these systems are referred as spinons with spin $= 1/2$. As a result of the integrability of the $S = 1/2$ Heisenberg spin chains, intrinsic spinon-spinon coupling alone is not resistive for magnetic heat transport according to theoretical calculations [6,7]. The expected divergence of the intrinsic 1D magnetic thermal conductivity (κ_m) makes the 1D spin chain an intriguing model system to study the celebrated Fermi-Pasta-Ulam-Tsingou problem [8,9] of nonlinear dynamics in 1D systems. It is thus encouraging that a high magnetic contribution to the thermal conductivity (κ) has been measured in several 1D magnetic systems with strong exchange interactions [10,11]. In these experiments, the finite κ_m is attributed to extrinsic spinon coupling with defects [12–15], grain boundaries [16], and other quasiparticles such as phonons [13,17,18] and charge carriers [19,20]. Thus, thermal transport measurements provide a useful probe of fundamental spinon transport length scales and coupling mechanisms, which cannot be readily obtained from other established methods. Meanwhile, for the spinon-induced SSE that was observed recently in the spin chain Sr_2CuO_3/Pt hybrid structure [3,4], the SSE signal was found to be decreased by impurities in Sr_2CuO_3 due to the suppression of spin transport, and an unusual temperature dependence of the SSE was further attributed to spinon-phonon coupling [4]. The importance of extrinsic spinon coupling mechanisms in both magnetic heat transport and SSE has motivated theoretical investigations [21–23]. In contrast to empirical expressions for spin-phonon coupling [24], recent theoretical studies have suggested a relatively weak upper bound for spinon-phonon coupling in the $S = 1/2$ Heisenberg spin chains [22,25]. However, experimental determinations of spinon-phonon coupling have been hindered by the lack of knowledge of the defect concentration, which was often taken as an adjustable fitting parameter [26], and the difficulty to separate κ_m and the lattice thermal conductivity (κ_l), the latter of which had to be assumed to be isotropic in several previous studies of κ_m in the anisotropic systems [12,24,27].

In this Letter, we present experiments that are designed to quantify extrinsic spinon coupling with defects and phonons in the $S = 1/2$ Heisenberg spin chain compound Ca_2CuO_3, the thermal transport properties of which had not been studied previously. The defect concentration due to chain breaking is obtained from the measured specific heat (C_p), an approach that has not been used in previous studies of spinon thermal transport. Based on recent progress in accurate first-principles calculations of the thermal properties [28], first-principles phonon dispersions and κ_l calculations are employed here to allow for the determination of the temperature-dependent spinon mean free paths (MFPs) due to defect scattering and phonon scattering via a kinetic model of 1D spinon thermal transport. The obtained temperature dependence of the MFP provides experimental support of the recent theory [25] of weak spinon-optical phonon coupling, which has important implications for both spinon heat transport and spinon-driven SSE.

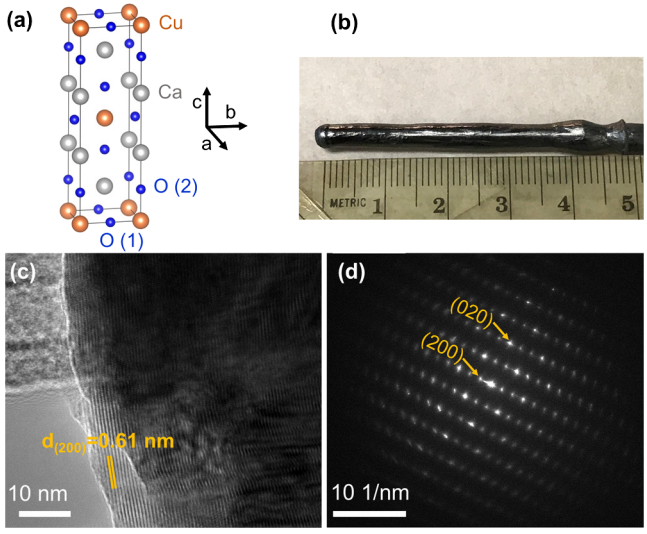

FIG. 1. (a) Crystal structure of Ca_2CuO_3. (b) A photo of a Ca_2CuO_3 crystal grown by the TSFZ method. (c) TEM image of the Ca_2CuO_3 crystal. (d) The corresponding selected area electron diffraction pattern of Ca_2CuO_3 in (c) obtained along the [001] zone axis.

Single crystals of Ca_2CuO_3 have been grown by the traveling-solvent floating zone (TSFZ) method [29]. The crystal structure of Ca_2CuO_3 and an image of one of the crystals are shown in Figs. 1(a) and 1(b), respectively. The material contains 180° Cu-O-Cu chains along the b axis with a strong antiferromagnetic coupling energy J/k_B of ~2000 K [43], where k_B is the Boltzmann constant. Figures 1(c) and 1(d) show a high-resolution transmission electron microscopy (TEM) micrograph and electron diffraction pattern of the crystal, respectively. The lattice spacing is found to be about 0.61 nm, in good agreement with the d value of the (200) plane in Ca_2CuO_3.

Figure 2(a) shows the Raman spectrum of Ca_2CuO_3 excited by 488 nm light at room temperature. The observed peak positions agree well with previous Raman studies [44–46]. The higher energy peaks with frequencies larger than 685 cm^{-1} are due to multiphonon scattering. The

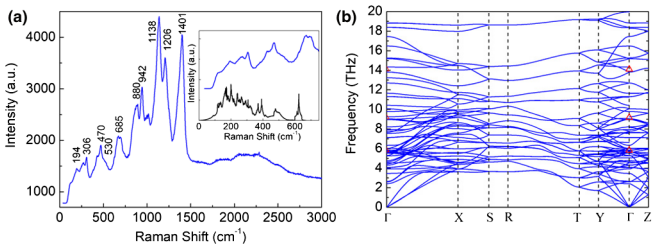

FIG. 2. (a) The measured Raman spectrum of Ca_2CuO_3 at room temperature. The inset shows the Raman spectrum (blue curve) in comparison with the phonon density of states from *ab initio* calculations (black curve). (b) Calculated phonon dispersion of Ca_2CuO_3. The red triangles are the measured Raman frequencies at 194, 306, and 470 cm^{-1}.

magnetic excitation in 1D antiferromagnetic Heisenberg chains is a continuum with a lower bound described by a des Cloizeaux–Pearson dispersion, $E(k) = \frac{1}{2}\pi J|\sin(k)|$, and a higher bound given by the triplet excitation dispersion, $E(k) = \pi J|\sin(\frac{1}{2}k)|$, where E and k are the energy and wave vector of spinons, respectively [44]. The spinon continuum extends over a range from zero to over 6000 cm^{-1}, as indicated by the humplike background in the Raman spectra. A broad peak is also observed around 2200 cm^{-1}, which is similar to the spinon-spinon pair states as reported in Sr_2CuO_3 [47]. The interaction between the continuum of spinons and discrete optical phonon states leads to Fano asymmetric line shapes in some high-energy two-phonon peaks, such as the one at 1401 cm^{-1}.

To calculate the phonon dispersion of Ca_2CuO_3, we combine a set of harmonic force constants obtained by a finite-difference method with a nonanalytic correction to the dynamical matrix [29,48]. Figure 2(b) shows the resulting phonon bands, plotted along a path passing through a representative set of high-symmetry points in the Brillouin zone. A particularly interesting feature of the dispersion is the clean folding of the bands at the boundaries along the b axis (Γ-Y), without clear evidence of symmetry breaking, e.g., the formation of minigaps. In other words, the effect of the lowered symmetry due to the magnetic order on the phonon bands is not remarkable. This fact provides support for our use of this dispersion even above the Néel temperature later on. In addition, the calculated phonon density of states is qualitatively consistent with the measured Raman spectra, as shown in the inset in Fig. 2(a).

Figure 3(a) shows the temperature dependence of C_p for Ca_2CuO_3. The lattice contribution (C_l) to the C_p is obtained from the calculated phonon dispersion [29]. The calculated value agrees well with the experimental data except at the very low temperature range, as shown in Fig. 3(a). Below ~4 K, the difference between the calculated and experimental data is due to the magnetic contribution.

At low temperatures, the C_p in the electrically insulating Ca_2CuO_3 consists of C_l and a contribution from magnetic excitations (C_m) as [27]

$$C_p(T) = C_l + C_m = \frac{12xN_A\pi^4k_B}{5}\left(\frac{T}{\theta_D}\right)^3 + \frac{2yN_Ak_B^2}{3}\left(\frac{T}{J}\right), \quad (1)$$

where N_A is Avogadro's constant, T is the temperature, θ_D is the Debye temperature, x is the number of atoms per formula unit, and y is the number of magnetic atoms per formula unit. The fitting of low-T C_p in the 6–15 K range according to Eq. (1) is shown in Fig. 3(b). The estimated θ_D of Ca_2CuO_3 is about 521 K, which is larger than the value of 448 K for Sr_2CuO_3 [49].

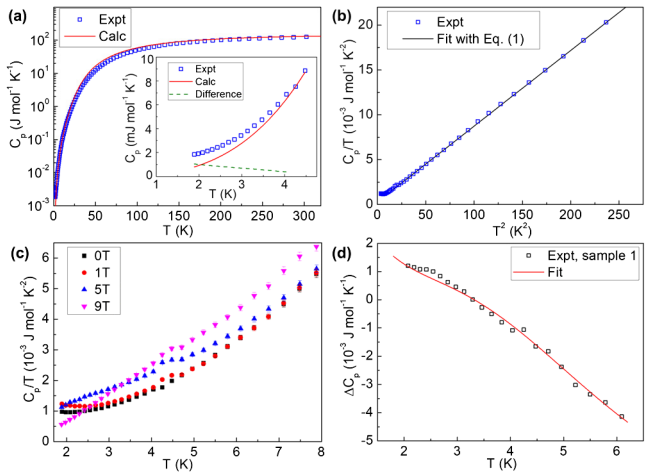

FIG. 3. (a) Temperature dependence of C_p for Ca_2CuO_3 in comparison with the calculated C_l based on phonon dispersion (red line). The inset is the difference between the calculated phonon contribution and measured C_p at low temperatures. (b) A plot of $C_p(T)/T$ vs T^2. The black line is the fitting curve according to Eq. (1). (c) $C_p(T)/T$ of a Ca_2CuO_3 crystal plotted as a function of the temperature under various applied magnetic fields. (d) Specific heat difference ΔC_p obtained by subtracting C_p of Ca_2CuO_3 under fields of 5 and 9 T. The red line is the fitting curve according to Eq. (2).

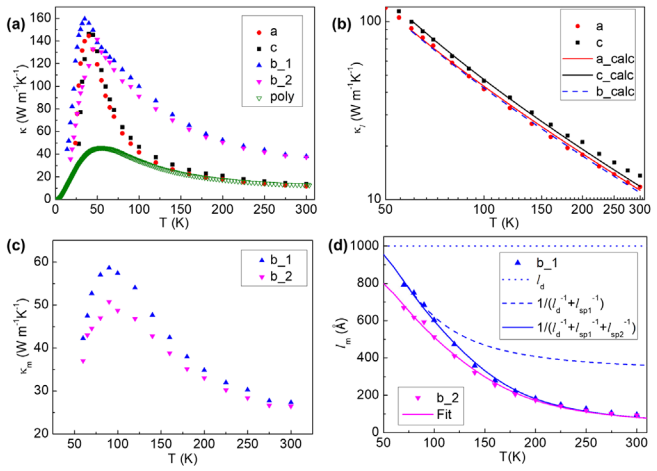

FIG. 4. (a) Thermal conductivity of Ca_2CuO_3 crystals measured along the three principal crystallographic axes, in comparison with the κ of a Ca_2CuO_3 polycrystalline sample. (b) Fit to the κ along the a and c axes. The blue dashed line is the calculated κ_l along the b axis. The details can be found in Supplemental Material [29]. (c) The extracted κ_m of Ca_2CuO_3 along the b axis. (d) Calculated spinon MFP of Ca_2CuO_3 along the b axis. The solid and dashed lines are the fits according to Eqs. (4)–(6).

Figure 3(c) shows the temperature dependence of C_p under various applied magnetic fields. There is an obvious upturn below 2.5 K observed in this sample and another sample [29] in the absence of the magnetic field. Such an anomaly could be caused by a Schottky contribution [49,50] due to the uncompensated spin 1/2 at the ends of fragmented chain segments. In the presence of defects, such as nonstoichiometry on copper or oxygen sites or impurity phases, 1D spin chains can break into even-length and odd-length segments, which have an even and an odd number of Cu sites, respectively. If the defect concentration is n_d, the average defect concentration due to the odd-length or even-length segments is about $0.5n_d$. The odd-length chains can introduce an additional contribution to C_p at low temperatures given by [51]

$$C_{\mathrm{Sch}} = (n_d/2)R(\Delta_g/T)^2 \exp(\Delta_g/T)/[1+\exp(\Delta_g/T)]^2, \quad (2)$$

where Δ_g is the energy level splitting and R is the ideal gas constant. To determine n_d, we analyzed the difference between the specific heat ($\Delta C_p = C_{p,H1} - C_{p,H2}$) measured at two different magnetic fields. Based on this method, the effect of lattice and spinon contributions can be minimized [50]. The ΔC_p data are fitted using the Schottky expression taking n_d and Δ_g under different magnetic fields as the fitting parameters, as shown in Fig. 3(d). The obtained fitting parameters are $n_d = 0.0039$ per Cu (0.001 Å^{-1}), $\Delta_g = 1.2$ K at 5 T, and $\Delta_g = 25$ K at 9 T for sample 1. The sensitivity analysis and the C_p results for sample 2 can be found in Supplemental Material [29].

The κ of the Ca_2CuO_3 crystals have been measured along all three crystallographic axes by a steady-state method [29], as shown in Fig. 4(a). The κ perpendicular to the spin chains (κ_a and κ_c) show similar absolute values and temperature dependence. However, the κ along the chains (κ_b) are much larger, especially from 70 to 300 K. Because Ca_2CuO_3 is an insulator, the higher κ along the chains have to be attributed to either a larger κ_l along b, or magnetic excitations, as observed in other spin chain compounds $SrCuO_2$ and Sr_2CuO_3 [24,26,27]. In addition, the peak κ of a polycrystalline sample is suppressed due to grain boundary scattering of phonons and spinons, in agreement with recent thermal transport measurements of polycrystalline $Sr_{14}Cu_{24}O_{41}$ [16].

We use the *ab initio* phonon results to calculate the κ_l and separate the spinon contribution. To examine the intrinsic phonon transport behavior of the compound and remove the influence of the boundaries of our specific samples, we focus on the temperature range above ~70 K. In the Boltzmann transport framework, we first fit the κ along the a and c axes [29], along which any magnetic contribution should be negligible. The good agreement between the fitting model and the measurement data is shown in Fig. 4(b). The κ_l along the b axis was calculated using the obtained fitting parameters and phonon dispersion. Despite an anisotropic crystal structure, the obtained κ_l are relatively isotropic along the three axes. Figure 4(c) shows the obtained κ_m for two samples by

subtracting κ_l from κ. The κ_m is about 27 $W\,m^{-1}\,K^{-1}$ at 300 K and increases with a decreasing temperature until the appearance of a peak κ_m value of 50–60 $W\,m^{-1}\,K^{-1}$ at about 90 K.

We now determine the spinon MFP (l_m) by analyzing the κ_m. The κ_m in a 1D system can be expressed as $\kappa_m = \int c_{m,k} v_{m,k} l_{m,k} dk$, and v_m is the spinon group velocity, $v_m = \pi J b/2\hbar$, where b is the distance between the spins along the chains and $\hbar$ is the reduced Plank constant. For $k_B T \ll J$, the heat-carrying spinons exist in significant number only in the vicinity of the band minima [10,52]. Therefore, it is adequate to assume that $l_m = l_{m,k}$ in order to obtain a relation between the MFP of spinons and the κ_m of a 1D system as [26,53]

$$l_m = \frac{3\hbar}{\pi N_s k_B^2 T}\kappa_m, \tag{3}$$

where $N_s = 2/ac$ is the number of spin chains per unit area. In addition, the two-spinon continuum is not considered here, since most of the excited spinons exist in the vicinity of the band minima for temperatures below 300 K [10,52]. As shown in Fig. 4(d), l_m of Ca_2CuO_3 is about 800 Å at 70 K for sample 1, corresponding to about 210 lattice spacings of b. With an increasing temperature, l_m is reduced and approaches a constant value of ~100 Å at 300 K for both samples.

In the temperature range for this study, heat transport by spinons is mainly limited by the spinon-defect scattering and spinon-optical phonon scattering processes [25]. The J is a function of the Cu-Cu separation that can be perturbed by thermal lattice vibrations. This perturbation provides the mechanism for coupling phonons to the spinons [21]. A recent theory has expressed the MFP due to the spinon-phonon scattering (l_{sp}) as [25]

$$l_{sp}^{-1} = g_{sp}^2 \frac{2J}{k_B T a} \frac{1}{\sinh(2\pi\hbar\varpi_0/k_B T)}, \tag{4}$$

where g_{sp} is the spinon-phonon coupling constant and ω_0 is the frequency of the phonon mode.

In addition, spinons can also be affected by impurities, which perturb the superexchange coupling locally. In effect, the defects can act like breaches in the spin chain. The corresponding MFP is an average length of a defect-free chain, which is given by [25]

$$l_d^{-1} = n_d. \tag{5}$$

To model the MFP of spinons, we have combined spinon-phonon and spinon-defect scattering according to Matthiessen's rule as

$$l^{-1} = l_{sp}^{-1} + l_d^{-1}. \tag{6}$$

In addition, we have assumed that the spinons are scattered by two optical phonon modes: $\omega_{0,1} = 6.25$ THz and $\omega_{0,2} = 19.17$ THz [25]. In our analysis, these two frequency values are the representative average values determined according to the effect of phonon modes on the degrees of freedom of Cu atoms along the b axis [29]. The first mode represents a broad distribution of phonon energy (E) centered at $E/k_B = 300$ K. The latter corresponds to the stretching mode at $E/k_B = 920$ K. The solid lines in Fig. 4(d) are the fits of the l_m for Ca_2CuO_3. With $J/k_B = 2200$ K, the obtained optimum fitting parameters are n_d=0.00099 $Å^{-1}$, $g_{sp,1} = 0.023$, and $g_{sp,2} = 0.16$ for sample 1 and n_d = 0.0012 $Å^{-1}$, $g_{sp,1} = 0.025$, and $g_{sp,2} = 0.16$ for sample 2. Sensitivity analysis [29] shows that these are unique fits to the data. The larger n_d for sample 2 can explain its lower κ_m below ~150 K. The obtained n_d agrees well with the value of 0.001 $Å^{-1}$ derived from the C_p data. In comparison, prior experimental and theoretical studies [21,24,27] on analyzing the spinon-phonon scattering MFP assumed a $g_{sp} \geq 1$. Based on the perturbative treatment of spinon-phonon scattering, however, recent theoretical studies [22,25] indicate that the upper limit on the spin-phonon coupling in 1D cuprates is ~0.2. Our experimental findings are consistent with the recent theoretical work, confirming the relative weak coupling between spinons and phonons in 1D Heisenberg $S = 1/2$ spin chain compounds. Moreover, based on the calculated MFP due to different scattering processes, defect scattering is dominant below ~50 K, which can explain the suppressed SSE signal in low-purity Sr_2CuO_3 below ~50 K [4]. In comparison, the spinon scattering is mainly limited by phonon scattering above ~50 K. Despite its small coupling constant, the $\omega_{0,1}$ mode is more effective in scattering spinons than the $\omega_{0,2}$ mode below 100 K. The $\omega_{0,2}$ mode starts to play a more important role at higher temperatures.

These experiments and analysis yield quantitative insight into spinon coupling with defects and phonons in single crystals of Ca_2CuO_3, which is considered to be a model system for strongly anisotropic spin-1/2 Heisenberg antiferromagnets. Spin chain breaking due to the presence of defects results in the observed Schottky anomaly in C_p at a low temperature. The magnetic-field-dependent C_p indicates a defect concentration of 0.001 $Å^{-1}$. Meanwhile, the determination of κ_l from the phonon dispersion has enabled its separation from the measured κ to obtain the large magnetic contribution κ_m. Based on the knowledge of the defect concentration and κ_m, the spinon MFP is obtained from a kinetic model of 1D spinon transport, which decreases from ~800 Å at 70 K to ~100 Å at 300 K. The MFP results suggest that defect scattering is the leading mechanism below 50 K, while optical phonon scattering is dominant at a high temperature, and provide experimental support of the recent theory of weak spinon-phonon coupling. Moreover, the methods presented in this work can be applicable to probe fundamental length scales in other low-D magnetic systems.

This work was supported by U.S. Army Research Office (ARO) MURI Grant No. W911NF-14-1-0016. The phonon dynamics calculation was performed using HPC resources from Grand Équipement National de Calcul Intensif- Très Grand Centre de Calcul (GENCI-TGCC) (Project No. A0030910242). The SPS processing at The University of Texas at Austin was conducted with the instrument acquired with the support of NSF Grant No. DMR-1229131. The crystal growth and the specific heat measurement were made possible by using the facility supported by NSF through the Center for Dynamics and Control of Materials: an NSF MRSEC under Cooperative Agreement No. DMR-1720595.

*lishi@mail.utexas.edu

[1] M. Uehara, T. Nagata, J. Akimitsu, H. Takahashi, N. Môri, and K. Kinoshita, J. Phys. Soc. Jpn. **65**, 2764 (1996).
[2] J. Schlappa *et al.*, Nature (London) **485**, 82 (2012).
[3] D. Hirobe, M. Sato, T. Kawamata, Y. Shiomi, K.-i. Uchida, R. Iguchi, Y. Koike, S. Maekawa, and E. Saitoh, Nat. Phys. **13**, 30 (2017).
[4] D. Hirobe, T. Kawamata, K. Oyanagi, Y. Koike, and E. Saitoh, J. Appl. Phys. **123**, 123903 (2018).
[5] S. Sahling, G. Remenyi, C. Paulsen, P. Monceau, V. Saligrama, C. Marin, A. Revcolevschi, L. P. Regnault, S. Raymond, and J. E. Lorenzo, Nat. Phys. **11**, 255 (2015).
[6] X. Zotos, F. Naef, and P. Prelovsek, Phys. Rev. B **55**, 11029 (1997).
[7] F. Heidrich-Meisner, A. Honecker, D. C. Cabra, and W. Brenig, Phys. Rev. B **68**, 134436 (2003).
[8] E. Fermi, J. Pasta, and S. Ulam, Los Alamos National Laboratory Report No. LA-1940, 1955.
[9] J. L. Tuck and M. T. Menzel, Adv. Math. **9**, 399 (1972).
[10] C. Hess, Eur. Phys. J. Spec. Top. **151**, 73 (2007).
[11] A. V. Sologubenko, T. Lorenz, H. R. Ott, and A. Freimuth, J. Low Temp. Phys. **147**, 387 (2007).
[12] A. Mohan, N. S. Beesetty, N. Hlubek, R. Saint-Martin, A. Revcolevschi, B. Büchner, and C. Hess, Phys. Rev. B **89**, 104302 (2014).
[13] N. Hlubek, P. Ribeiro, R. Saint-Martin, A. Revcolevschi, G. Roth, G. Behr, B. Büchner, and C. Hess, Phys. Rev. B **81**, 020405(R) (2010).
[14] C. Hess, B. Büchner, U. Ammerahl, L. Colonescu, F. Heidrich-Meisner, W. Brenig, and A. Revcolevschi, Phys. Rev. Lett. **90**, 197002 (2003).
[15] C. Hess, P. Ribeiro, B. Büchner, H. ElHaes, G. Roth, U. Ammerahl, and A. Revcolevschi, Phys. Rev. B **73**, 104407 (2006).
[16] X. Chen, K. Jarvis, S. Sullivan, Y. Li, J. Zhou, and L. Shi, Phys. Rev. B **95**, 144310 (2017).
[17] C. Hess, C. Baumann, and B. Büchner, J. Magn. Magn. Mater. **290**, 322 (2005).
[18] M. Montagnese *et al.*, Phys. Rev. Lett. **110**, 147206 (2013).
[19] C. Hess, H. ElHaes, B. Büchner, U. Ammerahl, M. Hücker, and A. Revcolevschi, Phys. Rev. Lett. **93**, 027005 (2004).
[20] A. V. Sologubenko, K. Gianno, H. R. Ott, U. Ammerahl, and A. Revcolevschi, Phys. Rev. Lett. **84**, 2714 (2000).
[21] A. L. Chernyshev and A. V. Rozhkov, Phys. Rev. B **72**, 104423 (2005).
[22] A. L. Chernyshev and W. Brenig, Phys. Rev. B **92**, 054409 (2015).
[23] K. Louis, P. Prelovšek, and X. Zotos, Phys. Rev. B **74**, 235118 (2006).
[24] N. Hlubek, X. Zotos, S. Singh, R. Saint-Martin, A. Revcolevschi, B. Büchner, and C. Hess, J. Stat. Mech. (2012), P03006.
[25] A. L. Chernyshev and A. V. Rozhkov, Phys. Rev. Lett. **116**, 017204 (2016).
[26] A. V. Sologubenko, K. Giannò, H. R. Ott, A. Vietkine, and A. Revcolevschi, Phys. Rev. B **64**, 054412 (2001).
[27] A. V. Sologubenko, E. Felder, K. Giannò, H. R. Ott, A. Vietkine, and A. Revcolevschi, Phys. Rev. B **62**, R6108 (2000).
[28] J. Carrete, B. Vermeersch, A. Katre, A. van Roekeghem, T. Wang, G. K. H. Madsen, and N. Mingo, Comput. Phys. Commun. **220**, 351 (2017).
[29] See Supplemental Material at http://link.aps.org/supplemental/10.1103/PhysRevLett.122.185901 for more details on synthesis methods, phase and microstructure characterization, specific heat and thermal conductivity measurements, first-principles calculations of phonon dispersion and lattice thermal conductivity, projected phonon density of states, fat-bands plot, and sensitivity analysis, which includes Refs. [30–42].
[30] J. Wada, S. Wakimoto, S. Hosoya, K. Yamada, and Y. Endoh, Physica (Amsterdam) **244C**, 193 (1995).
[31] H. Dang-Chinh, N. Duc-The, and H. Nam-Nhat, J. Phys. Condens. Matter **19**, 106215 (2007).
[32] N. C. Hyatt, L. Gray, I. Gameson, P. P. Edwards, and S. Hull, Phys. Rev. B **70**, 214101 (2004).
[33] G. Simutis *et al.*, Phys. Rev. B **95**, 054409 (2017).
[34] X. Chen, S. N. Girard, F. Meng, E. Lara-Curzio, S. Jin, J. B. Goodenough, J. S. Zhou, and L. Shi, Adv. Energy Mater. **4**, 1400452 (2014).
[35] W. Schnelle, R. Fischer, and E. Gmelin, J. Phys. D **34**, 846 (2001).
[36] G. Kresse and J. Hafner, Phys. Rev. B **47**, 558 (1993).
[37] G. Kresse and J. Furthmüller, Phys. Rev. B **54**, 11169 (1996).
[38] G. Kresse and J. Furthmüller, Comput. Mater. Sci. **6**, 15 (1996).
[39] G. Kresse and D. Joubert, Phys. Rev. B **59**, 1758 (1999).
[40] J. P. Perdew, K. Burke, and M. Ernzerhof, Phys. Rev. Lett. **77**, 3865 (1996).
[41] W. Tang, E. Sanville, and G. Henkelman, J. Phys. Condens. Matter **21**, 084204 (2009).
[42] A. Togo and I. Tanaka, Scr. Mater. **108**, 1 (2015).
[43] K. Foyevtsova, J. T. Krogel, J. Kim, P. R. C. Kent, E. Dagotto, and F. A. Reboredo, Phys. Rev. X **4**, 031003 (2014).
[44] S. Sugai, J. Wada, K. Yamada, S. Hosoya, and Y. Endoh, Physica (Amsterdam) **219B–220B**, 505 (1996).
[45] M. Yoshida, S. Tajima, N. Koshizuka, S. Tanaka, S. Uchida, and S. Ishibashi, Phys. Rev. B **44**, 11997 (1991).
[46] N. N. Hoang, D. C. Huynh, T. T. Nguyen, D. T. Nguyen, D. T. Ngo, M. Finnie, and C. Nguyen, Appl. Phys. A **92**, 715 (2008).

[47] O. V. Misochko, S. Tajima, C. Urano, H. Eisaki, and S. Uchida, Phys. Rev. B **53**, R14733 (1996).
[48] Y. Wang, J. J. Wang, W. Y. Wang, Z. G. Mei, S. L. Shang, L. Q. Chen, and Z. K. Liu, J. Phys. Condens. Matter **22**, 202201 (2010).
[49] K. Karmakar, R. Bag, M. Skoulatos, C. Rüegg, and S. Singh, Phys. Rev. B **95**, 235154 (2017).
[50] A. P. Ramirez, S. W. Cheong, and M. L. Kaplan, Phys. Rev. Lett. **72**, 3108 (1994).
[51] J. G. Cheng, J. S. Zhou, J. B. Goodenough, Y. T. Su, Y. Sui, and Y. Ren, Phys. Rev. B **84**, 104415 (2011).
[52] N. Hlubek, Magnetic heat transport in one-dimensional quantum antiferromagnets, Ph.D. thesis, Technische Universität Dresden, 2010.
[53] C. Hess, H. ElHaes, A. Waske, B. Büchner, C. Sekar, G. Krabbes, F. Heidrich-Meisner, and W. Brenig, Phys. Rev. Lett. **98**, 027201 (2007).